ELSEVIER

Journal of Structural Geology 27 (2005) 1011–1026

JOURNAL OF STRUCTURAL GEOLOGY

www.elsevier.com/locate/jsg

Flow perturbations: a tool to study and characterize heterogeneous deformation

Cees W. Passchier[a,*], Neil S. Mancktelow[b], Bernhard Grasemann[c]

[a]*Department of Geosciences, University of Mainz, Mainz 55099, Germany*
[b]*Department of Earth Sciences, ETH, CH-8092 Zurich, Switzerland*
[c]*Department of Geological Sciences, University of Vienna, Austria*

Received 30 July 2004; received in revised form 13 December 2004; accepted 27 January 2005
Available online 13 June 2005

Abstract

The classification of the myriad of small-scale structures that are used in tectonic analysis is presently based on their geometry, which makes it difficult to discover transitions and groups amongst them. An alternative would be to classify structures according to the flow type by which they form, but this is difficult. Although most structures form by heterogeneous flow, modelling studies are often focussed on bulk homogeneous flow, since the mathematical treatment of heterogeneous flow is cumbersome. Also, heterogeneous deformation patterns seem to occur in as many types as there are small-scale structures.

This paper introduces the use of the geometry of *flow perturbations* to improve our understanding of heterogeneous flow, and to allow classification of structures based on kinematics. A flow perturbation is the deviation of a heterogeneous flow pattern from the background homogeneous flow. Perturbation patterns can be visualised as open or closed loops of vectors, which occur in pairs, rows or groups of four. They usually cross-cut rheological interfaces, and can be subdivided into those that cross interfaces twice or four times. Most geological structures belong to the first group, while initiating buckle folds belong to the second group.

Keywords: Flow; Deformation; Perturbation; Shear zone

1. Introduction

Because of the slow progress of deformation in rocks, structural geology is the only science working with deforming materials that bases most of its attention on the final shape of deflected markers, known as deformation structures. Deformation structures in rocks are permanent changes in the geometry of older fabric elements such as layering or intrusive fabrics. They are either studied from a topical point of view in order to understand their development, or used as tools to reconstruct larger scale deformation processes, up to the scale of orogenesis. In such reconstructions, the development mechanism for particular small-scale structures is used to reconstruct flow and deformation at a larger scale based on the assumption that flow close to a small-scale feature is representative of a larger volume of surrounding material (Wallis, 1992; Simpson and de Paor, 1993; Beam and Fisher, 1999). An important problem in structural geology, however, is the myriad of different shapes that occur in nature. Nearly every structure is unique in some sense, and classification of structures is exceedingly difficult. Nevertheless, some sort of classification is useful if structures are to be used as tools in geological reconstructions. Many studies have therefore attempted, with variable success, to subdivide deformation structures observed in nature into groups with specific labels such as folds, shear bands, boudins or porphyroclasts (Passchier and Trouw, 1996). This approach is similar to classification systems of taxonomy in biology or palaeontology, where it is the shape of an organism that determines its place in a classification system. However, organisms with similar shape are not necessarily related, and structures with similar shape did not necessarily all form in the same way. In biology, DNA sequencing can now demonstrate the

* Corresponding author. Address: Department of Earth Sciences (Institut fuer Geowissenschaften), Johannes Gutenberg University, Tektonophysik, Becherweg 21, Mainz 55099, Germany. Tel.: +49 6131 392 3217.
E-mail addresses: cpasschi@uni-mainz.de (C.W. Passchier), jsg@mail.uni-mainz.de (C.W. Passchier).

0191-8141/$ - see front matter © 2005 Elsevier Ltd. All rights reserved.
doi:10.1016/j.jsg.2005.01.016

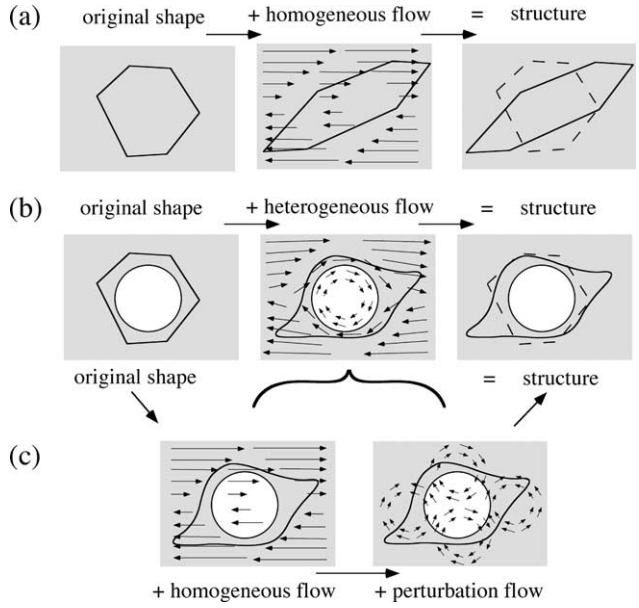

Fig. 1. Deformation structures in rocks can form by (a) homogeneous flow, or (b) heterogeneous flow. Heterogeneous flow can be regarded as (c) the sum of a homogeneous flow and a flow perturbation pattern.

relationship between organisms in a more reliable way, but in geology only an understanding of the progressive development mechanisms and histories can provide a reliable classification of related structures. Obviously, this is not always practical in the field where only final shapes are visible, but with the growing ability to model structures in analogue experiments and numerically, classification systems based on genesis are becoming viable. In this paper we propose a classification of structures in rocks based on the geometry of the flow pattern that produces them, rather than on their final shape. This different point of view could give as many surprises in geology as DNA-based taxonomy did in biology.

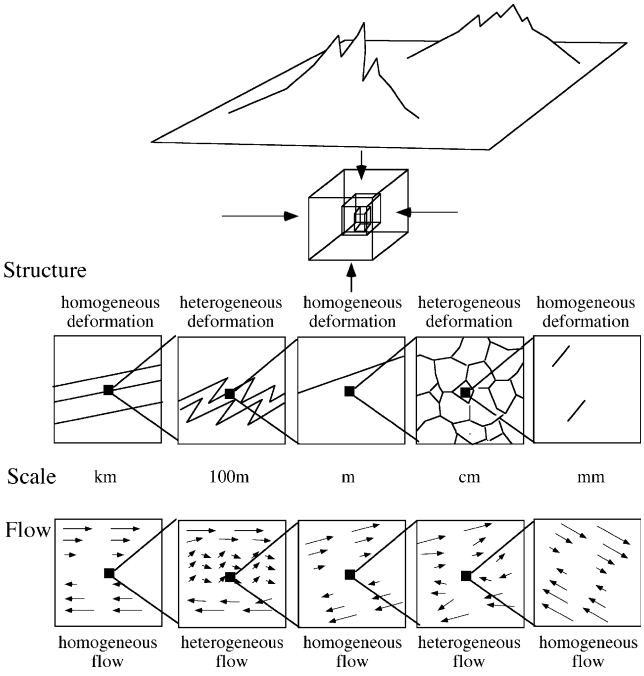

Fig. 2. Deformation that is studied at different scales in different observation volumes is commonly heterogeneous, but usually observation volumes can be found where flow and deformation are approximately homogeneous.

2. Flow and deformation perturbations

Many analytical studies of deformation in rocks have been based on the assumption of homogeneous flow such as pure-, simple- or general shear, which has the same geometry in any part of a material and at any scale exceeding that of individual grains (Fig. 1a). Such homogeneous flow can be considered in terms of either the velocity gradient or the deformation tensor for kinematic descriptions, which are mathematically easy to present, and give satisfactory results. Quite complex steady-state homogeneous flow and deformation can be described with just four constant parameters in two dimensions or nine in three dimensions, which are valid throughout a certain volume of rock (e.g. Ramberg, 1975; Passchier, 1988; Tikoff and Fossen, 1993).

Unfortunately, the concept of homogeneous flow and deformation is purely theoretical and not ideal for all materials and scales of observation. In many fluids, the concept of homogeneous flow and deformation is a good approximation at the micrometre to metre scale. However, unlike fluids, the rheology of rocks is notoriously heterogeneous and anisotropic on all scales and this induces heterogeneous flow and deformation (Fig. 1b). In geology, one tries to overcome this problem by imagining certain scales of observation where flow and deformation are approximately homogeneous (Means, 1976; Fig. 2). If the size of an ‘observation volume’ of material is gradually increased from micrometre to kilometre scale, several stages show material behaviour that could be approximately described as homogeneous. The reason is that at some scales of observation, deviations from the mean flow patterns are so small that they can be neglected (Fig. 2). This is the basis for justifying the application of homogeneous flow models to deforming rocks.

Some important types of structures do indeed form by homogeneous deformation in rheologically homogeneous rocks. Examples are many foliations and lineations, many deformed fossils and reduction spots, and some types of folds that form by passive amplification of non-planar layering (Fig. 1a). These structures are formed by an interplay between the bulk flow and some pre-existing shape(s) or marker surface(s) in the rock. Ironically, nearly *all* other structures, including the most important ones for structural geologists such as buckle folds, boudins, shear bands, shear zones, mullions, mantled porphyroclasts, veins, fringes and flanking folds (Coelho et al., in press), *cannot* form in homogeneous flow and deformation, but *need*

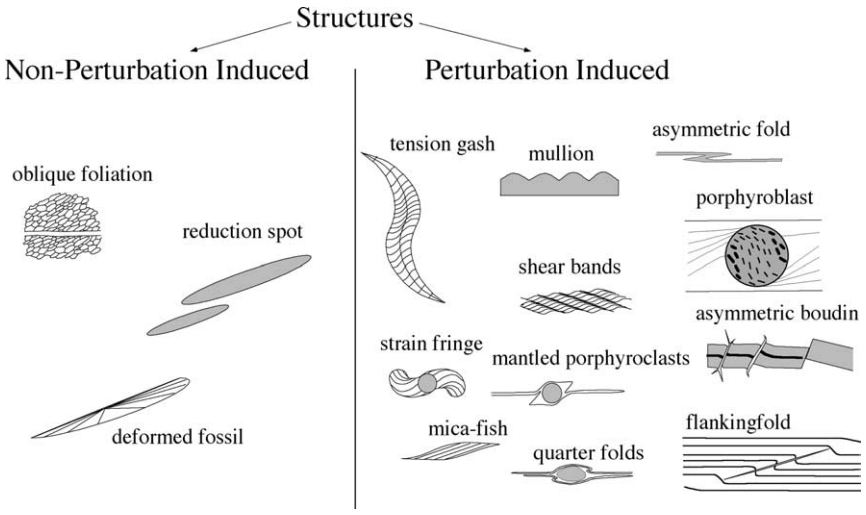

Fig. 3. Small-scale structures can be subdivided into a few that form by homogeneous flow, without flow perturbations, and a majority that needs flow perturbations for their development.

heterogeneous flow for their development (Fig. 1b). This is a reflection of rheological heterogeneities during their development. Heterogeneous rheology within a volume of rock is either original, due to variation in mineral or chemical composition, or induced (and changing) during the deformation process by hardening or softening. Data from a 'heterogeneous flow stage', e.g. the flow around a porphyroclast in a mylonite with an observation volume of ca. 1 cm^3, are then commonly used to infer flow conditions for the background homogeneous flow on a scale one to four orders of magnitude larger, e.g. the observation volume for a mylonite zone of ca. 1 m^3 (Fig. 2). Such 'upscaling projection' is the basis of all kinematic interpretation in structural geology.

Inhomogeneous flow or deformation is difficult to describe analytically, since the constants of the deformation tensors must be replaced by functions and strain parameters have to be obtained by derivation of the deformation gradient tensor. However, some heterogeneous kinematic analytical descriptions of rock deformation have been attempted (e.g. Hobbs and Talbot, 1966; Hobbs, 1971; Ramsay and Lisle, 2000). Analytical studies that have attempted to deal with heterogeneous deformation caused by rheologically inhomogeneous rock volumes (e.g. more competent clasts or layers in a less competent matrix) are even less numerous for the simple reason that this is much more complex mathematically, and needs more parameters to describe (e.g. Muskhelishvili, 1953; Biot, 1961; Fletcher, 1977; Smith, 1977; Schmid and Podladchikov, 2003). Commonly the solutions are restricted to infinitesimal deformation and approximated to first order, although fold initiation and amplification have been analysed up to third order (Johnson and Fletcher, 1994) and to finite amplitudes (Schmalholz and Podladchikov, 2000), with correspondingly complex solutions.

In this paper we have decided to try another approach to deal with heterogeneous flow or deformation. We consider the geometry of heterogeneous flow or deformation to be a vector addition of a homogeneous vector field, and perturbations to this homogeneity (Fig. 1c). The shape of these perturbations usually changes with time and development of the structure. As in the concept of incremental and finite deformation in a homogeneous flow, one can imagine infinitesimal and finite deformation perturbations superimposed on a homogeneous background flow or deformation (e.g. Cobbold, 1975; Mancktelow, 1991). Infinitesimal perturbations will be different at different times during the deformation process, and the finite deformation perturbation will be the addition of all these incremental ones. In this paper, only the instantaneous (or infinitesimal) perturbation flow field is treated in order to illustrate the concept. Based on these considerations, structures in rocks can be basically divided into non-perturbation induced and perturbation induced structures (Fig. 3). Flow perturbations occur on many scales, but in this paper we concentrate on those that occur on the same scale as the structures studied, in practice on the millimetre to tens of metres scale.

3. The perturbation flow field

The perturbation flow field is a vector field, involving both magnitude and direction (Figs. 1c and 4). It is defined at every point by the actual velocity minus the background velocity expected for either homogeneous or heterogeneous flow[1] with the imposed boundary conditions. The definition is instantaneous and can only reflect the boundary

[1] An example of a predefined heterogeneous background flow is that developed in a ring shear machine, where the shear strain rate decreases radially outwards (e.g. Arbaret et al., 2001).

conditions, geometry of rheological boundaries and rheology at any instant. From the spatial gradient in the perturbation velocity, the perturbation rate of deformation can also be calculated throughout the model. For linear rheology (e.g. linear elasticity or viscosity), the total velocity field is a linear superposition of the background and perturbation components, which can therefore be treated independently. This is the basis for analytical solutions describing, for example, the translation of a particle through a fluid (Batchelor, 1967) or fold initiation and growth (Fletcher, 1974, 1977). For the sake of simplicity and to highlight the principles of the method, this work only discusses examples of perturbation velocities where the background deformation induced by the boundary conditions is homogeneous, and more specifically either pure or simple shear.

The pattern of a perturbation flow field is determined only by the geometry of rheological boundaries in the observed volume of material, and on boundary conditions. Changes in the magnitude of rheological parameters (e.g. viscosity) change the magnitude of the perturbation velocities but not the overall pattern (Batchelor, 1967). Isolated rheological heterogeneities (e.g. an inclusion as in Fig. 4) can only cause an isolated perturbation in the velocity field. The perturbation velocity field must therefore decrease in magnitude away from the heterogeneity, with the length scale provided by the size of the heterogeneity (Fig. 4b), and the vectorial trajectories form open or closed loops that can approach each other, but cannot cross (Fig. 4c). As the perturbation velocity field pattern depends only on the geometry of the rheological heterogeneity and the far-field flow, the system symmetry must also be present in the perturbation flow, allowing many simple patterns to be predicted a priori. In general, there will be points of zero perturbation at the centre of closed loops, analogous to *stagnation points* in bulk flow (Ottino, 1989; Passchier and Sokoutis, 1993), while different loops are separated by surfaces known as *separatrices* (Ottino, 1989; Passchier and Sokoutis, 1993; Fig. 4). Separatrices also join in points of zero perturbation velocity (e.g. the central point in Fig. 4a–d). However, it must be emphasized that material points follow streamlines defined by the total velocity field and not just the perturbation component. The perturbation flow fields do not have direct connotations for the movement of particles.

4. Examples of perturbation flow fields for common structures

4.1. Modelling methods

To investigate the geometry of flow perturbation fields, numerical experiments were performed using a personally developed (NM) finite-element code for incompressible viscous flow. The code uses 7-node triangular elements with seven internal integration points for the examples with isolated inclusions and 9-node quadratic elements with nine internal integration points for the single layer examples, in each case with linear (3-node) interpolation of pressure and elimination of pressure at the element level (e.g. Hughes, 2000; Zienkiewicz and Taylor, 2000). Incompressibility was enforced by Uzawa iteration (Arrow et al., 1958; Zienkiewicz and Taylor, 2000). Constant strain rate boundary conditions appropriate to pure or simple shear were imposed. In the pure shear experiments, the velocity on the converging boundaries was constrained and the diverging boundaries were left free. In the simple shear experiments, the upper and lower boundaries had imposed velocity constraints, whereas the left and right boundaries were periodic (i.e. the x velocity of corresponding points on the left and right boundaries was constrained to be the same, and the y velocity was set to zero). Patterns, for example, with circular or elliptical cross-sections were also calculated analytically (Fig. 4b and c; Muskhelishvili, 1953; Schmid and Podladchikov, 2003), in part as a check on the finite-element code. The instantaneous perturbation velocity patterns were calculated in each case by subtracting a bulk homogeneous flow appropriate to the boundary conditions from the observed inhomogeneous flow pattern (Figs. 4–10).

4.2. Isolated inclusions

Perhaps the simplest example of a perturbation velocity field is that of an isolated cylindrical inclusion (circular in cross-section) in plane strain. The salient characteristics of a perturbation velocity field are readily seen in Fig. 4: (1) the magnitude of the perturbation velocity field decreases away from the inclusion; (2) the pattern reflects the overall symmetry of the system (i.e. both inclusion and imposed background velocity field, in this case pure shear; cf. Paterson and Weiss, 1961); and (3) the vectorial directions form open or closed loops, which can be highlighted by drawing trajectories parallel to the perturbation vectors. If boundary conditions are the same, changing the sign of the background velocity field (i.e. from horizontal shortening as in Fig. 4 to horizontal extension) merely changes the sign of the perturbation velocity field but the pattern remains the same. This is obvious in Fig. 4 where switching the horizontal and vertical axes would have the same effect. As noted above, changing the magnitude of the rheological parameters (in this case viscosity) changes the magnitude but not the form of the perturbation velocity field. Inverting the viscosity ratio (i.e. from a strong to weak inclusion) also inverts the direction of the perturbation velocity vectors, but with the same magnitude (Fig. 4a and d), while perturbation velocities are obviously zero when the inclusion and the host material have the same viscosity. Perturbation velocities along the horizontal (x) and vertical (y) axes are also vertical and horizontal. The rotation rate of these directions is therefore the same as the imposed flow, namely zero, reflecting the fact that particles with circular cross-section do not rotate in pure shear.

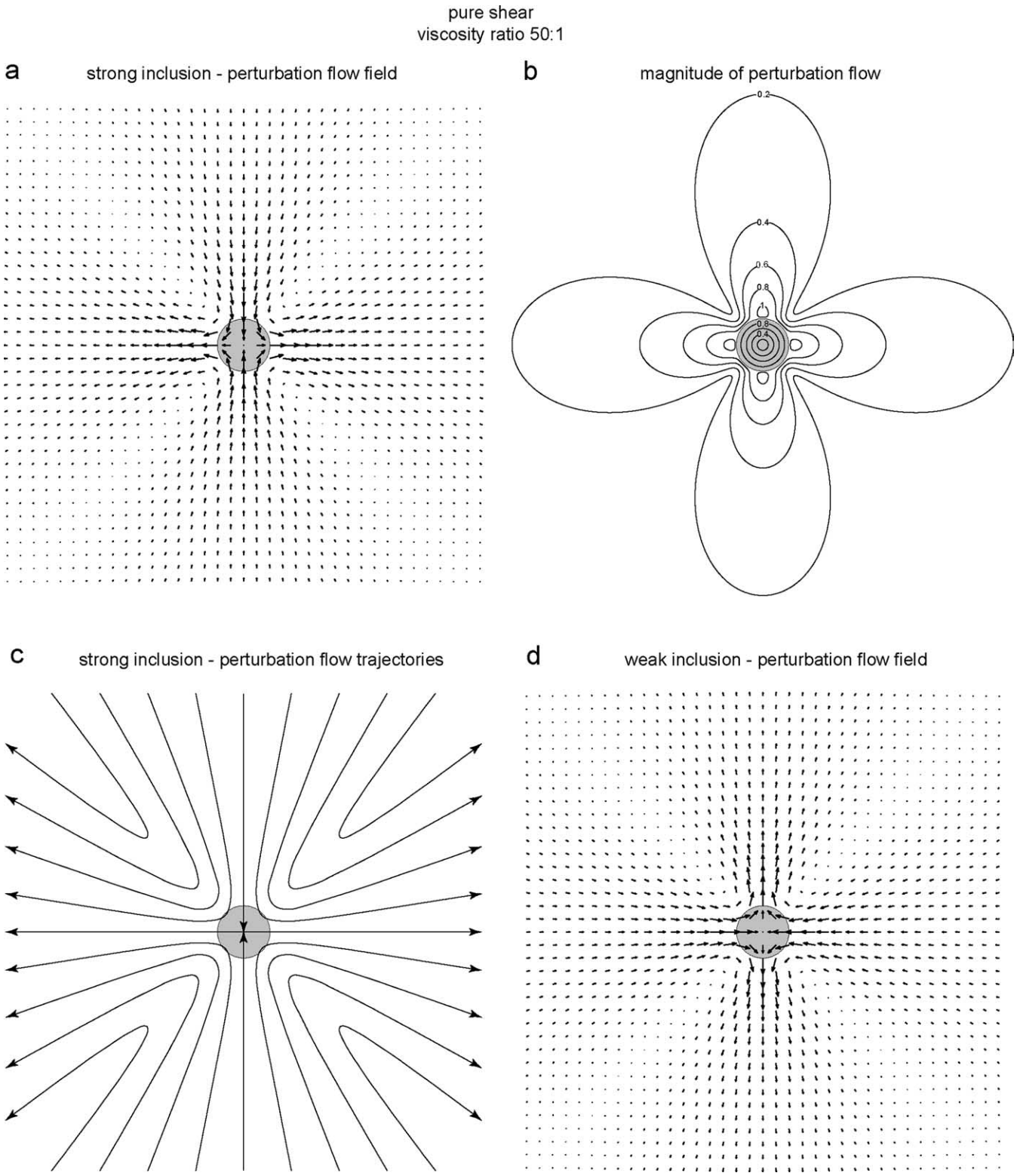

Fig. 4. Perturbation velocity flow fields around an isolated cylindrical particle (circular cross-section) in pure shear. Materials are incompressible linear viscous, with a viscosity ratio of 50:1. Shortening direction is horizontal. (a) Perturbation flow field for a strong inclusion; (b) contours of the magnitude of the perturbation velocity normalized against the velocity at the surface of the inclusion for homogeneous flow (i.e. particle radius times the background strain rate); (c) trajectories of the perturbation flow fields; note that the vertical and horizontal lines correspond to separatrices and the central point where they meet is a point of zero perturbation flow (and in this case, a true stagnation point of the bulk flow); (d) perturbation flow field for a weak inclusion. The plots of (a) and (d) are calculated with an incompressible viscous finite-element code; the plots of (b) and (c) are calculated with the analytical solution of Schmid and Podladchikov (2003). For (a) and (d), the width of the bounding box (with imposed velocity boundary conditions) in the x- and y-directions is 20 times the circle diameter. For the analytical solution, the boundaries are at infinite distance.

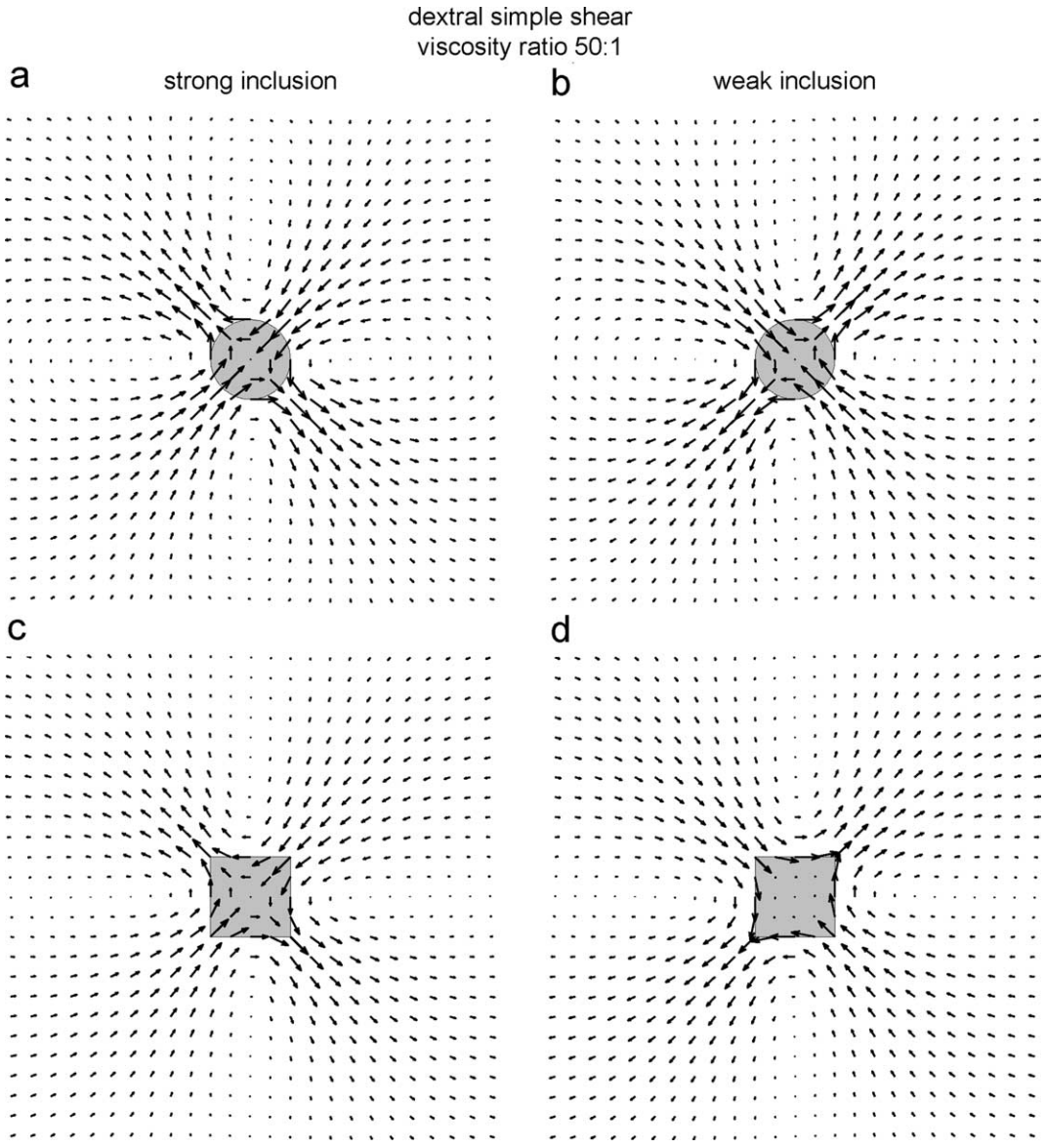

Fig. 5. Perturbation velocity flow fields around an isolated inclusion in dextral simple shear. Materials are incompressible linear viscous, with a viscosity ratio of 50:1. Shear direction is horizontal. In (a) and (b) the inclusion has a circular cross-section and the width of the bounding box in the *x*- and *y*-directions was 20 and 10 times the circle diameter, respectively. In (c) and (d) the inclusion has a square cross-section and the width of the bounding box in the *x*- and *y*-directions was five times the width of the inclusion. For (a) and (c) the inclusion is strong, in (b) and (d) it is weak.

Under simple shear (Fig. 5), the perturbation velocity is very similar but rotated by 45°, reflecting the different orientation of the instantaneous stretching axes (ISA). In this case, the particle does rotate, due to the rotational boundary conditions. The background flow causes a vertical passive line to rotate at the shear strain rate, whereas a horizontal line parallel to the shear direction does not rotate at all. A rigid equant particle therefore rotates at a rate equal to the average of these two extreme values, that is at half the shear strain rate. As a result, the perturbation velocity is tangential to the interface in the horizontal and vertical directions, with a magnitude of half the shear strain rate times the radius at the interface for a rigid inclusion. The direction is against the sense of shear in the vertical direction and with the sense of shear in the horizontal direction. Similar rules apply for stiff and weak inclusions subject to simple shear, as shown in Fig. 5. Reversing the shear sense or inverting the viscosity ratio (weak inclusion, Fig. 5b) simply reverses the sense of the perturbation velocity vectors. Provided the same symmetry and average elongation are maintained, a different detailed shape of the particle, e.g. a square or hexagonal cross-section instead of a circular one, makes no difference to the general pattern (Fig. 5c and d), consistent with the observation that the instantaneous rotational behaviour of rigid inclusions is not sensitive to details of shape (Willis, 1977; Arbaret et al.,

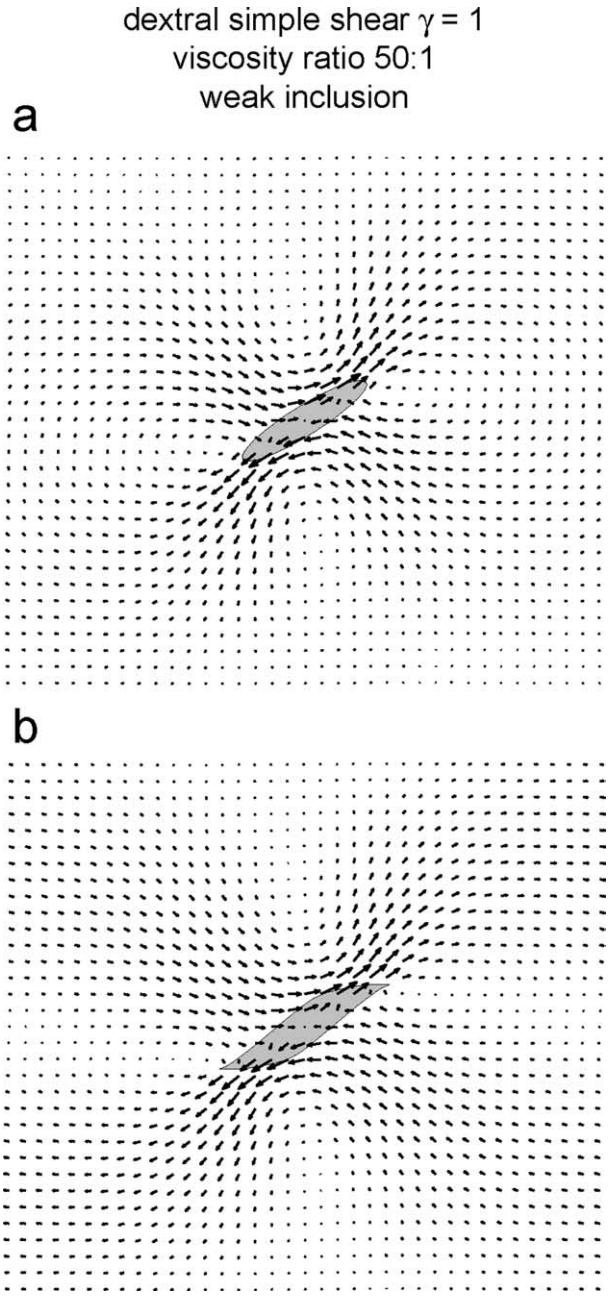

Fig. 6. Perturbation velocity flow fields for the weak particles of Fig. 5b and d after a dextral simple shear of $\gamma = 1$. Boundary conditions are the same as in Fig. 5.

2001). Notice that a change in the aspect ratio *does* have an influence on the pattern. The numerical models of Figs. 4 and 5 also illustrate the fact that the point and reflection symmetries of both the particle and the flow field relative to the ISA are reflected in the perturbation flow patterns (Paterson and Weiss, 1961).

In Fig. 6 the perturbation flow fields for elongate weak particles with initially circular or square cross-sections sheared to $\gamma = 1$ are presented. The differences in finite shape reflect the difference in the form of the initial particle outlines but the perturbation flow fields are again very similar, and the same applies to the continued development history. Examples will be presented below where this is not the case, and changes in shape of the rheological boundary with continued deformation eventually lead to very different patterns.

The consideration of hard and soft isolated inclusions has some interesting consequences (cf. Treagus and Lan, 2000, 2003, 2004). For example, in pure shear a passive marker circle deforms into an ellipse. In this case, the bulk flow is responsible and there are no flow perturbations. If the inclusion is softer than the matrix, stretching of the ellipse will be exaggerated; four flow perturbation cells exist which give the central particle an 'extra' deformation of the same style as the bulk flow (Fig. 4). In the opposite case, for a particle harder than the matrix, it will become less elliptical than the bulk strain ellipse; the perturbations work against the bulk flow. If the particle is rigid, the flow perturbation can be imagined to exactly balance the bulk flow inside the particle. Another way of imagining this is by instantaneous partitioning of homogeneous and perturbation components into two steps: the particle is deformed to an ellipse by homogeneous flow, but the perturbation pushes it back into its original shape.

4.3. Flanking folds

The perturbation flow fields around a weak particle with an elongate elliptical cross-section (20:1) are given in Fig. 7 for steps in orientation of 22.5°. This geometry is comparable to that considered by Grasemann and Stuwe (2001) and Grasemann et al. (2003) for the development of flanking structures around a weak cross-cutting element such as a shear zone or fault in bulk simple shear. As discussed above, a hard particle of the same shape would develop an identical perturbation flow pattern, but with the opposite sense. Four perturbation cells are still developed but in contrast to the equant particles, the separatrices are no longer perpendicular to each other and are unequally developed (Fig. 7). Comparison of Figs. 5–7 shows that with increasing ellipticity of an isolated particle, one set of two cells may decrease in significance at the cost of two other cells, but all four cells are in general still present. Based on these considerations, all weak or strong equidimensional and elliptical particles can be regarded as being associated with four perturbation cells, with transitions between them, although one pair of cells may be smaller and less pronounced. This implies that ductile shear zones, weak cylindrical particles, strong cylindrical particles and hard lenses are related structures in terms of their flow perturbations. In geological practice, this links mantled porphyroclasts, mineral fish, spiral garnets, flanking folds, shear bands, shear band cleavage, ductile shear zones and deformed enclaves as related structures.

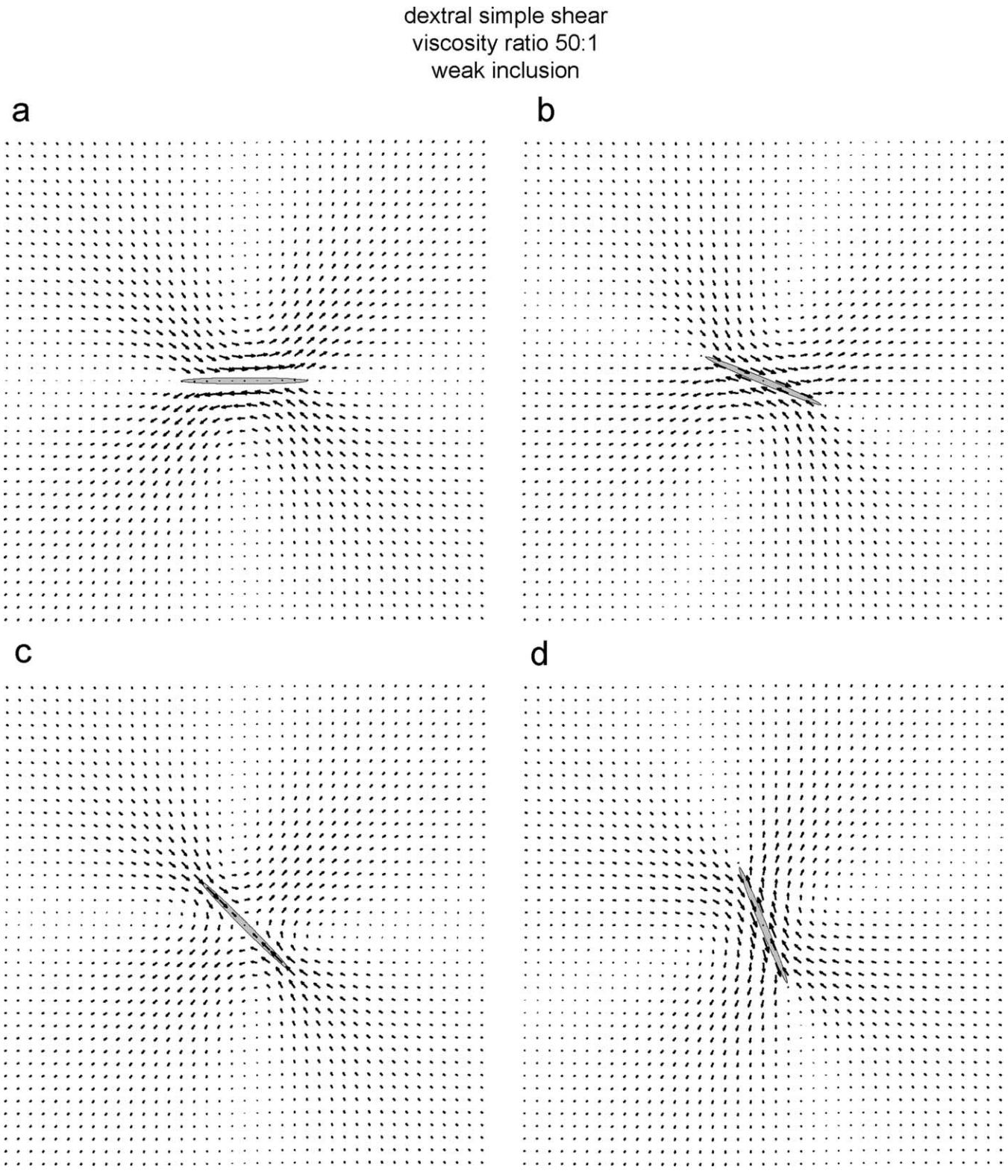

Fig. 7. Perturbation velocity flow fields in dextral simple shear for a weak particle with viscosity ratio 50:1 and an axial ratio 20:1 at different orientations of the particle. The angle between particle and a reference axis is increased from a–h in steps of 22.5°. The width of the bounding box is 16 times the maximum dimension of the ellipse in both the *x*- and *y*-directions.

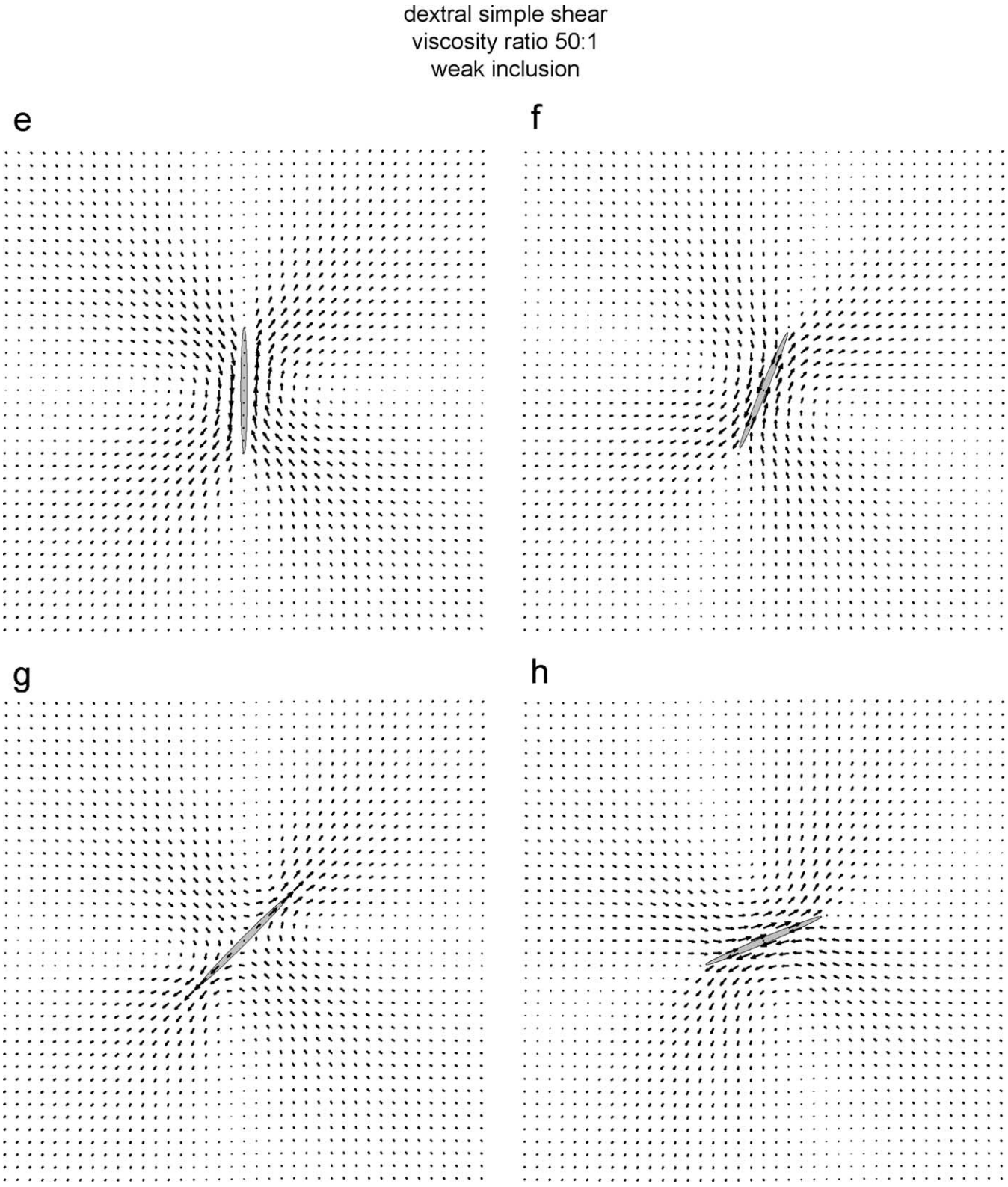

Fig. 7 (*continued*)

4.4. Layers

Rocks are commonly layered and shortening and extension of layering results in mechanical instability, an associated perturbation velocity field and, with time, the development of finite deformation structures such as folds, mullions or boudins (Smith, 1975, 1977). In all these cases, initial irregularities in the layer surface are amplified into

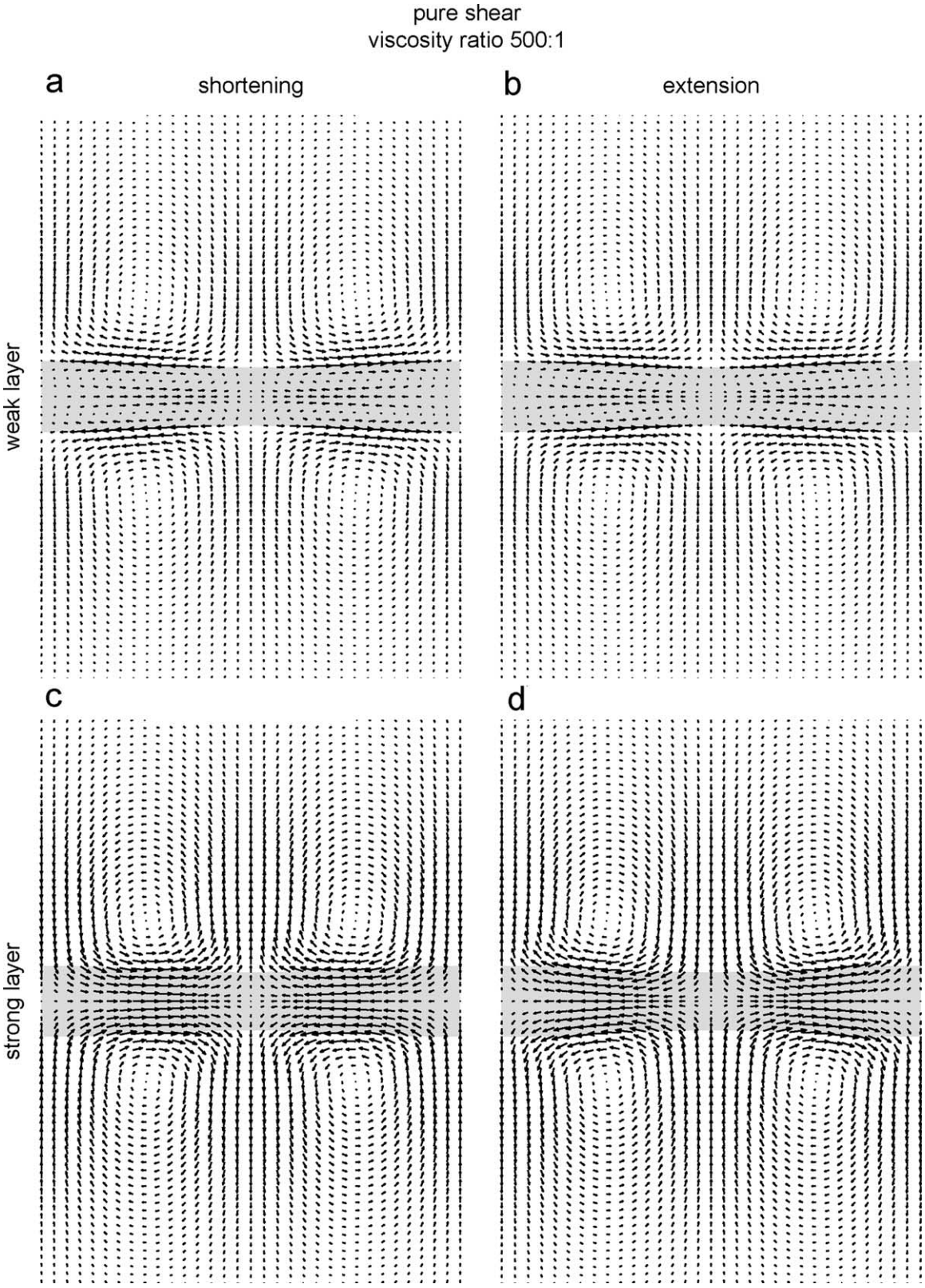

Fig. 8. Perturbation velocity flow fields for layer parallel shortening or extension with an antiphase sinusoidal variation with wavelength 6.5 times and amplitude 1/20 of the layer thickness. The width of the model box in the *y*-direction is initially 24 times the layer thickness and the upper and lower boundaries are left free. Viscosity ratio is 500:1.

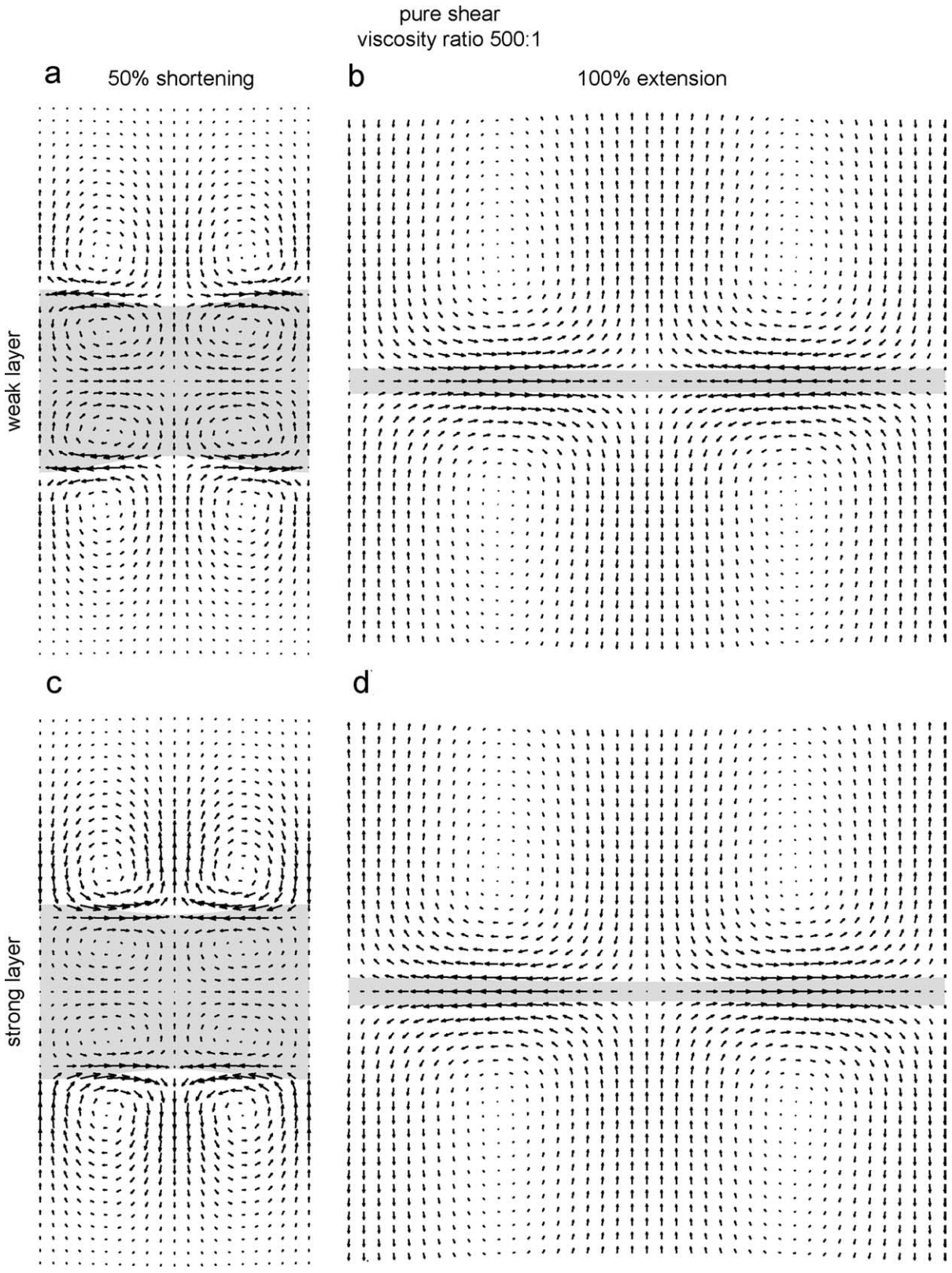

Fig. 9. Perturbation velocity flow fields after 50% shortening and 100% extension of the initial geometries of Fig. 8.

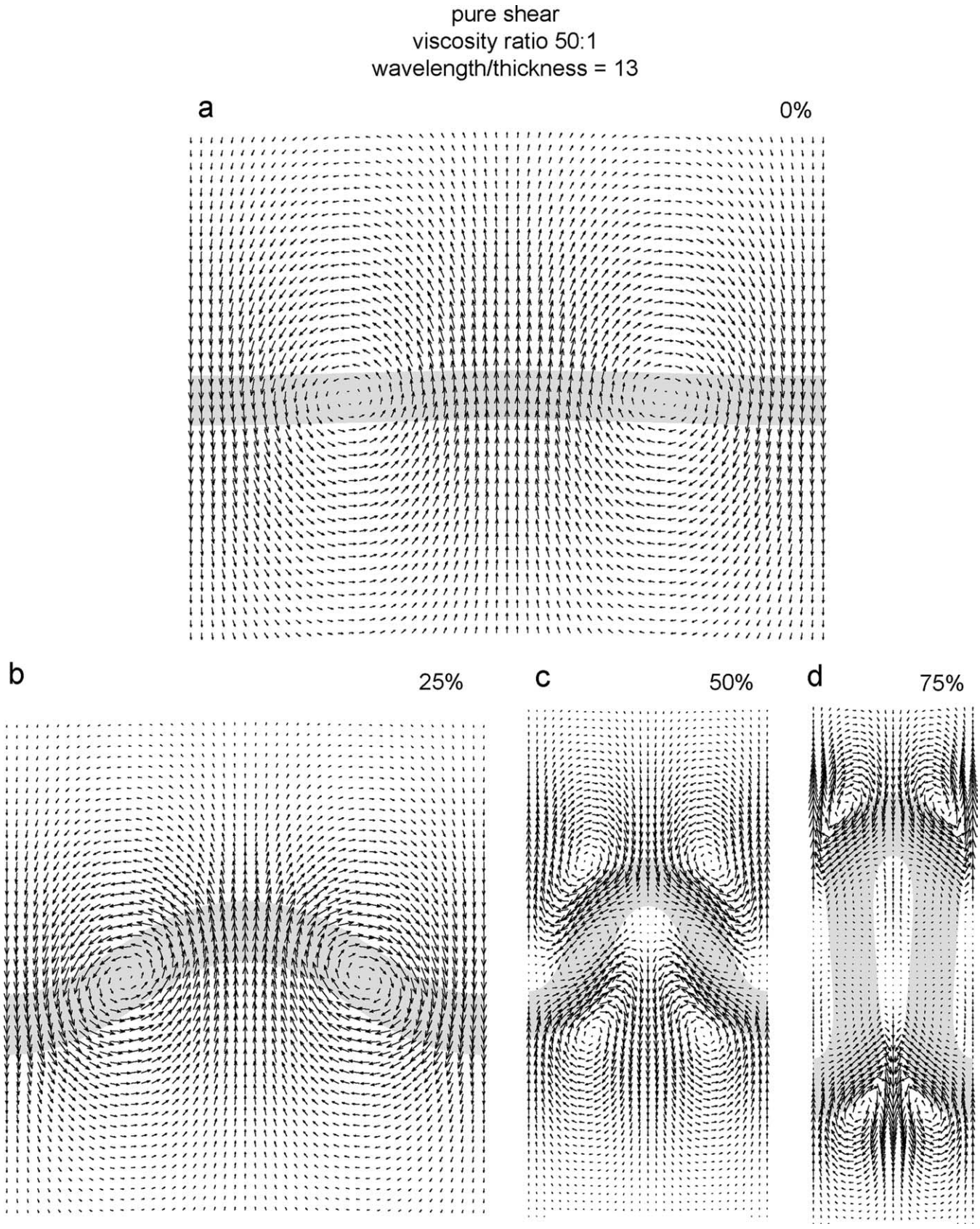

Fig. 10. Perturbation velocity flow fields for several stages of single layer buckle folding with viscosity ratio 50:1, wavelength 13 times layer thickness (ca. the fastest growing or 'dominant' wavelength), and initial amplitude 1/20 of layer thickness. The width of the model box in the *y*-direction is initially 100 times the layer thickness and the upper and lower boundaries are left free. Double intersection perturbation loops occur at initial stages of buckling, but these eventually split up into more usual single intersection perturbation loops.

finite structures as a result of the mechanical instability, with one particular wavelength (depending on layer thickness, viscosity contrast and material rheology) amplifying fastest—the so-called dominant wavelength (e.g. Biot, 1961; Fletcher, 1974, 1977; Smith, 1975, 1977; and many others). In most natural cases, the growth rate of the dominant wavelength will not be sufficient to completely swamp the effect of the initial layer irregularities (Abbassi and Mancktelow, 1990; Mancktelow, 1999, 2001). In detail, the perturbation flow field will then be unique for every combination of layer thickness, viscosity contrast, rheology and initial perturbation distribution. However, the general characteristics of instability development in layered material is better highlighted by only considering the developing dominant wavelength, and this is the approach followed here.

The initiation of mechanical instability for one end-member example of a single wavelength interface irregularity, namely an antiphase sinusoidal form, is considered in Fig. 8. The four possible combinations of shortening or extension of a strong or weak layer are shown. One complete wavelength segment is presented although, from symmetry, half the wavelength would be sufficient. Notice that, instead of four perturbation cells, we now have an unlimited number of perturbation cell-pairs along an infinitely long layer. Changing from extension to shortening again simply involves a reversal in the perturbation velocity vector directions. However, patterns are different for weak and strong layers. The weak layer shows four cells in each half-wavelength segment bounded at the layer interface and the central surface, respectively, whereas the strong layer has only two cells that show reflection symmetry about the central surface. Of the four potential structures (Fig. 8a–d), only extension of a strong layer (Fig. 8d) shows a perturbation velocity field that would amplify the initial irregularity to produce a recognizable deformation structure at finite strain (a 'boudin'). For a weak layer (Fig. 8a and b), the perturbation velocity at the thickest and thinnest points on the layer surface is zero and there is no dynamic amplification. For shortening of a strong layer (Fig. 8c), the perturbation velocity field actually tends to deamplify the initial irregularity. The passive background flow will amplify the initial sinusoidal irregularity in shortening and deamplify it in extension. In summary, mullions (Fig. 8a) may develop by passive amplification at high finite strain, but without any help from dynamic amplification. Extension of a weak layer (Fig. 8b) will passively deamplify the initial irregularity. There is no dynamic contribution and therefore no structure would be expected to develop. Passive and dynamic effects work against each other in the case of shortening of an antiphase, sinusoidal layer thickness variation in a strong layer (Fig. 8c). For extension of a stronger layer (Fig. 8d), boudins may develop if the dynamic amplification is sufficient to overcome passive deamplification.

Fig. 9 shows the same initial set-ups as in Fig. 8 but now shortened by 50% or extended by 100%. After this deformation, the geometry of a layer that has been shortened is obviously very different from one that has been extended. However, for layers that have been either shortened or extended, there is no major difference between strong or weak layers. As a result, except for the expected reversal in direction, the patterns are practically identical (compare Fig. 9a with c and b with d). These numerical experiments also show how difficult it is to develop boudins in linear viscous materials, even when the viscosity contrast is high (500:1 in the case considered here). This is known from superplastic behaviour in material science. As the rheological behaviour approaches that of linear viscosity (typically attained in fine-grained metals and ceramics, for which diffusion becomes the rate-controlling process), rods can be pulled to very high strains (extensions of 1000% or more, e.g. Poirier, 1985, pp. 204–212) without necking and 'boudin' development. Natural boudin development is only possible for strongly non-linear viscous (Smith, 1977) and/or pressure-sensitive rheology (Strömgård, 1973).

Fig. 10 considers the classic case of buckle folding due to shortening of a stronger layer with an initial in-phase sinusoidal interface deflection. The perturbation velocity field highlights the changes that occur during progressive folding. Initially, dynamic amplification involves a rigid rotation of the limbs, reflected in single circular cells centred on the inflection points (Fig. 10a). With increasing amplitude, this single cell becomes more elongate (Fig. 10b) and as the limb rotates into an orientation of incremental stretching, three separate cells develop for each fold limb, the central one of which is still centred on the inflection point (Fig. 10c). At still higher shortening, the limb region around the inflection point and adjacent matrix stretches more-or-less homogeneously with the background flow as the hinge regions separate. The perturbation flow fields in the hinge regions become increasingly independent of each other, with one strong and one weak cell on each side of the hinge (Fig. 10d). This is a particularly good example in which the perturbation flow field highlights changes in the kinematics and dynamics of a process during its progressive development.

5. Classification of structures by perturbation flow geometry

Flow perturbation patterns in all experiments are open or closed loops (or cells) with high perturbation flow velocities near rheological interfaces, and more reduced flow perturbation velocities in the far-field matrix. In many cases, flow perturbation loops occur in pairs of different sense ('clockwise' or 'anti-clockwise') with separatrix planes in between.

Fig. 11 is a first attempt to classify structures according to their flow perturbation geometries. The scheme can be modified and further expanded as more experimental data

on more types of structures become available. Flow perturbation loops basically occur in three types, depending on the way in which they intersect rheological interfaces. Most perturbation loops and the separatrices between them cross a single rheological interface once (in-and-out). These we name *single transection perturbation* (*SIP*)-*loops*. Rarely, as in the case of initiating buckle folds, perturbation loops intersect two rheological interfaces. These we name *double intersection perturbation* (*DIP*)-*loops* (Fig. 11).

As discussed above, isolated objects such as ductile shear zones, weak and strong cylindrical particles and hard lenses are characterised by four open SIP-perturbation loops arranged in a cross-shape. For effectively circular cross-sections, the two arms of the cross are perpendicular and the cells are all equally developed. For increasingly elongate particles, two cells may come to dominate but all four cells are still present.

From the patterns in Figs. 8 and 9 discussed above, it is also clear that mullions, boudins and pinch-and-swell structures form a single family of related structures with SIP-loops, connected by transitions in perturbation geometry (cf. Smith, 1975, 1977). Basically, they are similar in shape to the family of isolated particles described before (Figs. 4 and 5). Buckle folds, however, are interesting because they show DIP-loops in their initial stages of development (Fig. 10a), which later split into SIP-loops centred on the rheological interfaces in the hinge-zones (Fig. 10d).

One interesting aspect is that in the classification of Fig. 11, perturbation geometry is strongly influenced by particle aspect ratio, and also to a lesser extent by particle orientation with respect to the instantaneous stretching axes (ISA) of the homogeneous background flow. Rheology contrast is of minor significance, and mainly determines the strength and sign of the perturbation field. In other words, it is the symmetry of the system that exerts the dominant control (Paterson and Weiss, 1961). Finally, the geometry of the homogeneous background flow, i.e. extension, contraction, sinistral or dextral simple shear, which is normally the core of classifications of flow and deformation, plays *no* significant role in the geometry of flow perturbations, and therefore has no effect on the classification based on these perturbations.

6. Discussion

In Fig. 11 we have not yet considered changes in the shape of flow perturbation patterns with time. In some structures such as rigid porphyroclasts, flow perturbation patterns may change little with time, while in others, such as buckle folds, the patterns are strongly modified with progressive development of the structure. Further experimental work could therefore allow a more detailed or alternative subdivision of structures into those with constant and variable flow perturbation patterns. Variable flow perturbation patterns could be further subdivided into (1) those that form around a pre-existing rheological contrast in

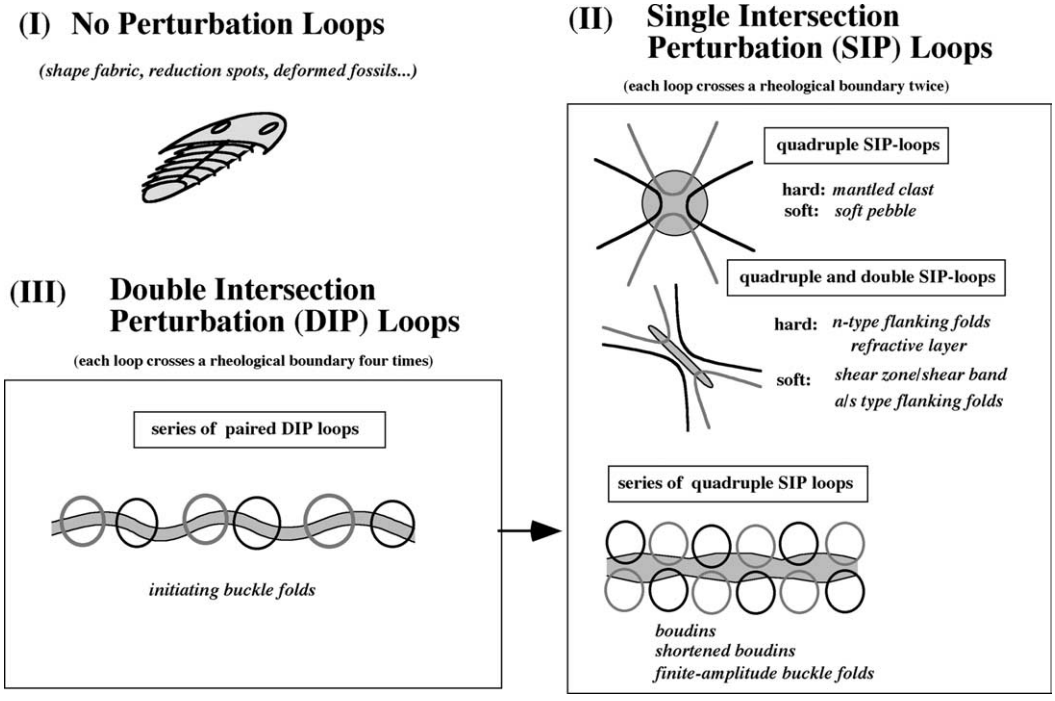

Fig. 11. First attempt to classify structures based on the types of flow perturbations observed during their development. Grey and black loops indicate the outline of perturbation velocity flow fields of opposite direction. The actual direction (sinistral or dextral) depends on viscosity contrast. The type of loops is described in boxes, while the associated structures are given in italics. Flanking fold terminology according to Coelho et al. (in press).

the rock, such as a layer or clast that does not change with time; (2) those that form around objects with a rheological contrast that changes with time, for example by hardening or softening; and (3) perturbation patterns that develop in rocks that initially have a homogeneous rheology but then undergo local hardening, softening or fracture.

We have concentrated in the current study on ductile deformation structures without volume change, and associated flow perturbations. The principle may equally be applied, however, to brittle deformation. In that case, a brittle fault or joint will normally coincide with a flow separatrix, as can be seen from Fig. 7, where an elongate weak inclusion could be taken as an approximation for a discrete brittle fracture. In the case of volume change or erosion, flow perturbation cells in the solid material will be open and have more complex shapes than discussed here.

In this paper, we have only discussed flow perturbations, which are by definition instantaneous. As mentioned above, it might also be interesting to study deformation perturbations, i.e. the perturbations of a structure from the imaginary results of homogeneous deformation (Mancktelow, 1991, fig. 6). For example, it may be instructive to plot the difference in the position of particles between a folded layer and the same layer if it had shortened and thickened homogeneously. At first sight, this would be an obvious method to classify structures, since deformation geometries can be observed without the need for experiments. There are, however, some problems with the use of deformation perturbations for structural classification: (1) it is commonly difficult to find with certainty a large number of material points of which the initial position is known; (2) the large displacement involved in finite deformation perturbations produces a confuse pattern of overlapping vectors; and (3) the genetic link to the underlying mechanics involved in the development of the structure is lost, because similar finite perturbation geometries may not necessarily indicate related structures in terms of their development.

Another aspect neglected so far is the 3D geometry of perturbation patterns. All the structures considered in this paper have a cylindrical geometry and the third dimension can therefore be ignored. However, when considering more complex objects, 3D flow perturbation patterns have to be modelled and investigated, although the principle will be the same as outlined above.

7. Conclusions

The perturbation velocity field, which can be readily calculated for analytical, numerical and analogue models of deformation structures, is a powerful tool for analysing the development of these structures. By considering the perturbation flow, similarities and differences can be highlighted and this may shed light on the kinematics of structure growth. The perturbation flow therefore also provides a rational basis for classification of deformation structures. Transitions and gradients in perturbation shape may help to find hidden links between apparently unrelated structures.

Acknowledgements

Thanks to the FLASH research team, in particular U. Exner, T. Kocher, G. Wiesmayr, and S. Coelho for many stimulating discussions. Y. Podladchikov is thanked for invaluable help in the initial stages of FEM code development and B. Kaus, G. Simpson and D. Schmid for important feedback. Matlab routines for calculating and plotting the analytical solution for flow around an isolated elliptical inclusion were modified from those of D. Schmid. Support for NM was provided by ETH project 0-20998-02. CWP acknowledges support from DFG grant no. 2220681. Thorough and constructive reviews by D. Jiang and P. Hudleston are also gratefully acknowledged.

References

Abbassi, M.R., Mancktelow, N.S., 1990. The effect of initial perturbation shape and symmetry on fold development. Journal of Structural Geology 12, 273–282.

Arbaret, L., Mancktelow, N.S., Burg, J.-P., 2001. Effect of shape and orientation on rigid particle rotation and matrix deformation in simple shear flow. Journal of Structural Geology 23, 113–125.

Arrow, K., Hurwicz, L., Uzawa, H., 1958. Studies in Nonlinear Programming. Stanford University Press, Stanford.

Batchelor, G.K., 1967. An Introduction to Fluid Dynamics. Cambridge University Press, Cambridge.

Beam, E.C., Fisher, D.M., 1999. An estimate of kinematic vorticity from rotated elongate porphyroblasts. Journal of Structural Geology 21, 1553–1559.

Biot, M.A., 1961. Theory of folding of stratified viscoelastic media and its implication in tectonics and orogenesis. Geological Society of American Bulletin 72, 1595–1620.

Cobbold, P.R., 1975. Fold propagation in single embedded layers. Tectonophysics 27, 333–351.

Coelho, S., Passchier, C.W., Grasemann, B. 2005. Geometric description of flanking structures. Journal of Structural Geology 27, 597–606.

Fletcher, R.C., 1974. Wavelength selection in the folding of a single layer with power-law rheology. American Journal of Science 274, 1029–1043.

Fletcher, R.C., 1977. Folding of a single viscous layer: exact infinitesimal-amplitude solution. Tectonophysics 39, 593–606.

Grasemann, B., Stuwe, K., 2001. The development of flanking folds during simple shear and their use as kinematic indicators. Journal of Structural Geology 23, 715–724.

Grasemann, B., Stuwe, K., Vannay, J.C., 2003. Sense and non-sense of shear in flanking structures. Journal of Structural Geology 25, 19–34.

Hobbs, B.E., 1971. The analysis of strain in folded layers. Tectonophysics 11, 329–375.

Hobbs, B.E., Talbot, J.L., 1966. The analysis of strain in deformed rocks. The Journal of Geology 74, 500–513.

Hughes, T.J.R., 2000. The Finite Element Method. Linear Static and Dynamic Finite Element Analysis. Dover, New York.

Johnson, A.M., Fletch, R.C., 1994. Folding of Viscous Layers. Columbia University Press, New York.

Mancktelow, N.S., 1991. The analysis of progressive deformation from an inscribed grid. Journal of Structural Geology 13, 859–864.

Mancktelow, N.S., 1999. Finite-element modelling of single-layer folding in elasto-viscous materials: the effect of initial perturbation geometry. Journal of Structural Geology 21, 161–177.

Mancktelow, N.S., 2001. Single-layer folds developed from initial random perturbations: the effects of probability distribution, fractal dimension, phase, and amplitude. In: Koyi, H.A., Mancktelow, N.S. (Eds.), Tectonic Modeling: A Volume in Honor of Hans Ramberg Geological Society of America Memoir, 193, pp. 69–87.

Means, W.D., 1976. Stress and Strain: Basic Concepts of Continuum Mechanics for Geologists. Springer, Heidelberg.

Muskhelishvili, N.I., 1953. Some Basic Problems of the Mathematical Theory of Elasticity. Noordhoff, Groningen.

Ottino, J.M., 1989. The Kinematics of Mixing. Stretching, Chaos and Transport. Cambridge University Press, Cambridge.

Passchier, C.W., 1988. Analysis of deformation paths in shear zones. Geologische Rundschau 77, 309–318.

Passchier, C.W., Sokoutis, D., 1993. Experimental modelling of mantled porphyroclasts. Journal of Structural Geology 15, 895–909.

Passchier, C.W., Trouw, R.A.J., 1996. Microtectonics. Springer, Berlin.

Paterson, M.S., Weiss, L.E., 1961. Symmetry concepts in the structural analysis of deformed rocks. Geological Society of America Bulletin 72, 841–882.

Poirier, J.P., 1985. Creep of Crystals. Cambridge University Press, Cambridge.

Ramberg, H., 1975. Particle paths, displacement and progressive strain applicable to rocks. Tectonophysics 28, 1–37.

Ramsay, J.G., Lisle, R.J., 2000. The Techniques of Modern Structural Geology, Applications of Continuum Mechanics in Structural Geology, vol. 3. Academic Press, London.

Schmalholz, S.M., Podladchikov, Y.Y., 2000. Finite amplitude folding: transition from exponential to layer length controlled growth. Earth and Planetary Science Letters 179, 363–377.

Schmid, D.W., Podladchikov, Y.Y., 2003. Analytical solutions for deformable elliptical inclusions in general shear. Geophysical Journal International 155, 269–288.

Simpson, C., de Paor, D., 1993. Strain and kinematic analysis in general shear zones. Journal of Structural Geology 15, 1–20.

Smith, R.B., 1975. Unified theory of the onset of folding, boudinage and mullion structure. Geological Society of America Bulletin 86, 1601–1609.

Smith, R.B., 1977. Formation of folds, boudinage, and mullions in non-Newtonian materials. Geological Society of America Bulletin 88, 312–320.

Strömgård, K.-E., 1973. Stress distribution during formation of boudinage and pressure shadows. Tectonophysics 16, 215–248.

Tikoff, B., Fossen, H., 1993. Simultaneous pure and simple shear: the unifying deformation matrix. Tectonophysics 217, 267–283.

Treagus, S.H., Lan, L., 2000. Pure shear deformation of square objects, and applications to geological strain analysis. Journal of Structural Geology 22, 105–122.

Treagus, S.H., Lan, L., 2003. Simple shear of deformable square objects. Journal of Structural Geology 25, 1993–2003.

Treagus, S.H., Lan, L.B., 2004. Deformation of square objects and boudins. Journal of Structural Geology 26, 1361–1376.

Wallis, S.-R., 1992. Vorticity analysis in a metachert from the Sanbagawa Belt, SW Japan. Journal of Structural Geology 14, 271–280.

Willis, D.G., 1977. A kinematic model of preferred orientation. Geological Society of America Bulletin 88, 883–894.

Zienkiewicz, O.C., Taylor, R.L., 2000. The Finite Element Method Volume 1: The Basis. Butterworth/Heinemann, Oxford.